A Hysteretic Model of Hydraulic Properties for Dual-Porosity Soils

Rudiyanto
Dep. of Civil and Environmental Engineering
Bogor Agricultural Univ.
Bogor, Indonesia

Nobuo Toride*
Masaru Sakai
Graduate School of Bioresources
Mie Univ.
Tsu, Mie, Japan 514–8507

Jiří Šimůnek
Dep. of Environmental Sciences
Univ. of California
Riverside, CA 92521

We propose a hysteretic model of hydraulic properties for dual-porosity soils based on the bimodal van Genuchten model and Kool and Parker (K&P) hysteresis model. Hysteresis is considered only in the first pore domain, affecting mainly higher water contents, while a nonhysteretic behavior is assumed in the second pore domain, affecting mainly lower water contents. The main drying and wetting curves are described with the same set of parameters except for α_1, which is different for the drying and wetting curves. The scanning hysteresis loops in the first subregion are also described using the K&P model. The hysteretic water retention model agrees reasonably well with drying and wetting retention curves and scanning loops observed for Andisols. Although the corresponding unsaturated hydraulic conductivity, evaluated using the Mualem pore-size distribution model, as a function of the water content, $K(\theta)$, is nonhysteretic for higher water contents, unrealistic hysteresis occurs in $K(\theta)$ for lower water contents. To obtain an "almost" nonhysteretic $K(\theta)$ function for the entire range of water contents, an additional constraint on the value of the α_1 parameter for $K(\theta)$ is imposed, and a single value is used for both drying and wetting curves.

Abbreviations: K&P, Kool and Parker; VG, van Genuchten.

Water retention in aggregated soils is often described as a dual-porosity (or bimodal) system consisting of inter- and intraaggregate pore domains, each having their own hydraulic properties. Durner (1992, 1994) developed a multimodal retention function as a summation of multiple van Genuchten (VG) models (van Genuchten, 1980) to describe a stepwise water retention curve. This function, which may be reduced to a bimodal function, has been used quite widely in recent years (e.g., Coppola, 2000; Peters and Durner, 2008; Schindler et al., 2010; Schelle et al., 2010, 2011; Durner and Iden, 2011; Diamantopoulos et al., 2012).

Miyamoto et al. (2003) applied the bimodal VG model to highly aggregated Japanese volcanic-ash soils, which exhibited a distinct stepwise water retention curve. Similar to the capillary water retention of coarse-textured sandy soils, hysteresis may also exist for water retained in interaggregate pores, which are represented by the first part of the bimodal water retention curve in the near-saturation range. Although remarkable hysteresis loops were observed in the retention curve near saturation for baked ceramic aggregates (Steinberg et al., 2005), only limited effort has been made to develop a hysteretic model for dual-porosity soils.

Kool and Parker (1987) proposed a hysteretic model based on the formulations introduced by Scott et al. (1983) for the unimodal VG model. The Kool and Parker (K&P) model describes the main drying and wetting curves using different

Soil Sci. Soc. Am. J. 77:1182–1188
doi:10.2136/sssaj2012.0339n
Received 8 Oct. 2012
*Corresponding author (ntoride@bio.mie-u.ac.jp)

values of the unimodal VG model parameter α. The K&P model estimates drying and wetting scanning curves based on the scaling of the main drying and wetting curves, respectively. Because it is relatively flexible in describing hysteretic loops, the K&P model is widely used in numerical water flow simulation codes such as HYDRUS (Šimůnek et al., 2008b), SWAP (Kroes et al., 2008), and UNSAT-H (Fayer, 2000), regardless of its simple assumptions and formulations. Minor modifications of the K&P model have been suggested by Lenhard et al. (1991) and Lenhard and Parker (1989) to eliminate the so-called "pumping," or unclosed hysteretic loops, by keeping track of historical reversal points.

The objective of this study was to introduce hysteretic water retention into the bimodal VG model based on the K&P model. The applicability of the proposed hysteretic model is demonstrated using observed hysteretic water retention curves and scanning curves for an Andisol. The unsaturated conductivity function based on the Mualem (1976) model is discussed for the main wetting and drying retention curves. We propose an additional constraint for a nonhysteretic hydraulic conductivity function when expressed as a function of the water content.

MATERIAL AND METHODS

Observed Hysteretic Water Retention Curves

Because of a well-developed and stable aggregate structure made up of noncrystalline minerals (e.g., allophane, imogolite, and ferrihydrite), Andisols exhibit unique physical properties such as a low bulk density, a high porosity, and a stepwise water retention curve reflecting inter- and intraaggregate pores (Miyamoto et al., 2003). Hysteretic water retention curves were observed for an Andisol from an upland field at the National Institute of Vegetable and Tea Science in Mie, Japan, using a multistep outflow–inflow experiment. The soil, sieved through a 2-mm mesh, was packed in a 5-cm-depth and 5-cm-diameter soil column at a bulk density of 0.75 g cm^{-3}. A fritted glass filter of a 6-mm thickness was used at the bottom of the soil column. The bottom pressure head was controlled using a Marriotte bottle during sample wetting and by decreasing the position of a drip point during draining. A tensiometer was horizontally installed at the 2.5-cm depth. Cumulative water inflow and drainage were monitored by regularly weighing the soil column.

After saturating the soil with a Marriotte bottle supply, the bottom pressure head was gradually decreased to −80.5 cm to obtain the main drying retention curve. After switching back to the Marriotte bottle supply, the main wetting retention curve was monitored by increasing the bottom pressure head to saturation. Draining and wetting processes were subsequently repeated in the intermediate pressure head range to obtain drying and wetting scanning curves. The average water contents of the soil column were determined based on the cumulative inflow and drainage and the final water content at the end of the experiment. Hysteretic water retention curves were obtained from the average water contents and the corresponding tensiometer readings. Figure 1 shows the collected hysteretic water retention curves as well as their fit using the hysteretic model described below.

Hysteretic Model

Dual-Porosity Hydraulic Functions

The dual-porosity retention function introduced by Durner (1992, 1994) is expressed as a linear superposition of the unimodal VG model for each subregion:

$$S=\frac{\theta(h)-\theta_r}{\theta_s-\theta_r}=w_1S_1+w_2S_2 \qquad [1]$$

in which S_i is given by

$$S_i=\left[1+\left(\alpha_i|h|\right)^{n_i}\right]^{-m_i} \qquad [2]$$

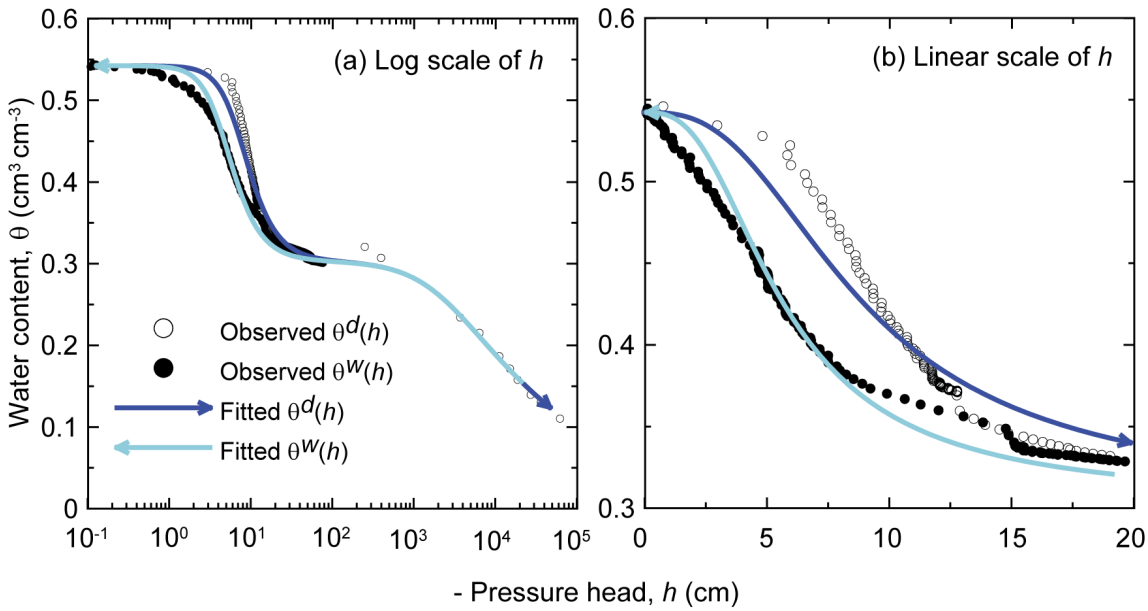

Fig. 1. Observed and fitted hysteretic water retention curves of the Mie Andisol on (a) a logarithmic scale of the pressure head, *h*, and (b) a linear scale of *h*. Observed drainage [$\theta^d(h)$] data points are displayed as open circles and observed wetting [$\theta^w(h)$] data points as solid circles. Dark blue lines represent drying curves and light blue lines represent wetting curves.

where the subscript i represents the subregion (i = 1 or 2), S is the effective saturation (dimensionless), h is the soil water pressure head [L], θ_s and θ_r are the saturated and residual water contents [L^3 L^{-3}], respectively, n_i (dimensionless), α_i [L^{-1}], and m_i ($= 1 - 1/n_i$) are shape parameters subject to $\alpha_i > 0$ and $n_i > 1$, and w_1 and w_2 are weighting factors subject to $0 < w_i < 1$ and $w_1 + w_2 = 1$. In the following discussion, S_1, subject to $\alpha_1 > \alpha_2$, corresponds with the first part of $\theta(h)$ in the higher water content range, while S_2 corresponds with the second part of $\theta(h)$ in the lower water content range. In the case of $w_2 = 0$, Eq. [1] is reduced to the unimodal VG model. A closed-form expression of the unsaturated hydraulic conductivity function for the dual-porosity retention function Eq. [1] based on the Mualem (1976) model was given by Priesack and Durner (2006):

$$K(\theta)=K_s\left(w_1S_1+w_2S_2\right)^{\ell}\times \frac{\left(w_1\alpha_1\left[1-\left(1-S_1^{1/m_1}\right)^{m_1}\right]+w_2\alpha_2\left[1-\left(1-S_2^{1/m_2}\right)^{m_2}\right]\right)^2}{\left(w_1\alpha_1+w_2\alpha_2\right)^2} \quad [3]$$

where K_s is the saturated hydraulic conductivity [L T^{-1}] and ℓ is a pore-connectivity coefficient (dimensionless). Hereafter, the dual-porosity hydraulic functions of Eq. [1–3] are referred to as the *bimodal VG model*.

Hysteretic Retention Functions

When $\theta_i(h)$ is defined as

$$\theta_i(h)=\left(\theta_s-\theta_r\right)w_iS_i+\theta_{ri} \quad [4]$$

the total water content in Eq. [1] can be simply expressed as a sum of three components:

$$\theta(h)=\theta_r+\left[\theta_1(h)-\theta_{r1}\right]+\left[\theta_2(h)-\theta_{r2}\right] \quad [5]$$

Because $\theta_{s1} - \theta_{r1} = (\theta_s - \theta_r)w_1$ and $\theta_{s2} - \theta_{r2} = (\theta_s - \theta_r)w_2$ for $h = 0$ in Eq. [4], the effective saturation of the ith subregion can be defined similarly to Eq. [1]:

$$S_i=\frac{\theta_i(h)-\theta_{ri}}{\theta_{si}-\theta_{ri}} \quad [6]$$

Because θ_r is independently defined, in addition to the water contents of the subregions in Eq. [5], θ_{ri} is assumed to be zero in this study.

Because Fig. 1 shows that hysteresis may occur only in the first, high-saturation part of the dual-porosity retention function, we apply the K&P model (Kool and Parker, 1987) to $\theta_1(h)$ while assuming nonhysteretic $\theta_2(h)$. The main hysteretic loop is described with $\alpha_1^{\,d}$ for the main drying curve, $\theta_1^{\,d}(h)$, and $\alpha_1^{\,w}$ for the main wetting curve, $\theta_1^{\,w}(h)$. The remaining parameters (θ_s, θ_r, n_1, w_2, α_2, and n_2) are the same for both curves.

Scanning Retention Curves

The K&P model is also applied to $\theta_1(h)$ to describe the scanning curves of $\theta(h)$. Drying scanning curves are scaled using the main drying curve, $\theta_1^{\,d}(h)$, and can be expressed as (Šimůnek et al., 2008a)

$$\theta_1(h)=\theta_{r1}+\alpha_{\theta1}\left[\theta_1^{d}(h)-\theta_{r1}^{d}\right] \quad [7]$$

where $\alpha_{\theta1}$ is the scaling factor for the drying scanning curve passing through the latest reversal point ($\theta_{\Delta1}$, h_Δ) from wetting to drying. The scaling factor $\alpha_{\theta1}$ is obtained by substituting ($\theta_{\Delta1}$, h_Δ) into Eq. [7] assuming $\theta_{r1} = \theta_{r1}^{\,d}$:

$$\alpha_{\theta1}=\frac{\theta_{\Delta1}-\theta_{r1}}{\theta_1^{d}(h_\Delta)-\theta_{r1}} \quad [8]$$

Note that we keep a nonzero θ_{r1} in the above scaling Eq. [7–8] despite assuming $\theta_{r1} = 0$. This is because a similar scaling procedure for wetting scanning curves based on the main wetting curve is used, as shown below. The scaling procedure results in a fictitious value of the parameter θ_{s1}^*, which can be obtained by substituting the full saturation point (θ_{s1}, 0) into Eq. [7] (Šimůnek et al., 2008a; Kool and Parker, 1987):

$$\theta_{s1}^*=\theta_{r1}+\alpha_{\theta1}\left(\theta_{s1}^{d}-\theta_{r1}\right)=\frac{\theta_{\Delta1}-\theta_{r1}\left[1-S_1^{d}(h_\Delta)\right]}{S_1^{d}(h_\Delta)} \quad [9]$$

Note that an identical drying scanning curve as in Eq. [7] can be derived by replacing θ_{s1} with θ_{s1}^* in the main drying curve described with Eq. [2] and [6] (Kool and Parker, 1987). Because the main hysteresis loop is closed at saturation, $\theta_{s1}^{\,d}$ and $\theta_{s1}^{\,w}$ are equal to θ_{s1}.

Similarly, wetting scanning curves are scaled using the main wetting curve, $\theta_1^{\,w}(h)$, and can be described as

$$\theta_1(h)=\theta_{r1}^*+\alpha_{\theta1}\left[\theta_1^{w}(h)-\theta_{r1}^{w}\right] \quad [10]$$

where θ_{r1}^* is the fictitious residual water content and $\alpha_{\theta1}$ is the scaling factor for a particular wetting scanning curve. Substituting the reversal point ($\theta_{\Delta1}$, h_Δ) and the full saturation point (θ_{s1}, 0) into Eq. [10] leads to

$$\theta_{\Delta1}=\theta_{r1}^*+\alpha_{\theta1}\left[\theta_1^{w}(h_\Delta)-\theta_{r1}^{w}\right] \quad [11]$$

$$\theta_{s1}=\theta_{r1}^*+\alpha_{\theta1}\left[\theta_{s1}^{w}-\theta_{r1}^{w}\right] \quad [12]$$

Subtracting Eq. [12] from Eq. [11] results in

$$\alpha_{\theta1}=\frac{\theta_{\Delta1}-\theta_{s1}}{\theta_1^{w}(h_\Delta)-\theta_{s1}^{w}} \quad [13]$$

The fictitious residual water content, θ_{r1}^*, can be obtained by substituting Eq. [13] into Eq. [12] (Šimůnek et al., 2008a; Kool and Parker, 1987):

$$\theta_{r1}^*=\theta_{s1}-\alpha_{\theta1}\left[\theta_{s1}^{w}-\theta_{r1}^{w}\right]=\frac{\theta_{\Delta1}-\theta_{s1}S_1^{w}(h_\Delta)}{1-S_1^{w}(h_\Delta)} \quad [14]$$

Table 1. Parameter values of the hysteretic bimodal van Genuchten model for two types of hypothetical soils having different n_1 values, and fitted parameter values for observed main drying and wetting retention curves for the Mie Andisol, including residual and saturated water contents (θ_r and θ_s, respectively), van Genuchten shape parameters (α^d for the drying cycle, α^w for the wetting cycle, and n), and a weighting factor (w) for the two subregions (subscripts 1 and 2).

Soil	θ_r	θ_s	α_1^d	α_1^w	n_1	w_2	α_2	n_2
	— m^3 m^{-3} —		— cm^{-1} —				cm^{-1}	
Soil with n_1 = 2.56	0	0.57	0.121	0.543	2.56	0.52	0.00035	1.3
Soil with n_1 = 1.20	0	0.57	0.121	0.543	1.2	0.52	0.00001	1.3
Mie Andisol	0	0.542	0.139	0.219	2.8	0.559	0.00047	1.29

Note again that a wetting scanning curve identical to that derived using Eq. [10] can be also derived by replacing θ_{r1} with θ_{r1}^* in the main wetting curve described with Eq. [2] and [6] (Kool and Parker, 1987). Also note that it is possible to formulate the scanning curve model to describe unclosed hysteretic loops, as done for the unimodal VG model by Lenhard et al. (1991) and Lenhard and Parker (1989).

RESULTS AND DISCUSSION

Main Wetting and Drying Branches of Hysteretic Retention Curves

Figures 1a and 1b show the observed hysteretic water retention curves on a logarithmic scale for $-10^{-1} > h > -10^5$ cm and on a linear scale for $0 > h > -20$ cm, respectively. Drying retention data measured with a pressure plate for $-100 > h > -1000$ cm and a dewpoint potentiometer (WP4, Decagon Devices) for $h < -1000$ cm are also plotted in Fig. 1a. The wetting curve data range between a pressure head of −76 cm and saturation. Because the drying and wetting curves practically merged for pressure heads below $h = -20$ cm (Fig. 1b), we assume that the observed retention curves can represent both the main drying and wetting curves, confirming our assumption made above that the distinct hysteretic behavior occurs only in the first part of the retention curve near saturation.

To test the hysteretic model, all data from the main drying and wetting curves including data for $h < -100$ cm in Fig. 1a were fitted simultaneously by minimizing the root mean square error between the fitted and observed data sets (RMSEθ) using the Solver add-in in Microsoft Excel. The parameters θ_s, α_1^d, α_1^w, n_1, w_2, α_2, and n_2 were optimized assuming $\theta_r = 0$ for the sake of simplicity (Durner, 1994). Figures 1a and 1b also show the main drying and wetting curves using optimized parameter values listed in Table 1. Because the water retention curve exhibits a distinct air entry near saturation with a steep gradient of $d\theta/dh$, n_1 is quite large (= 2.8); however, the fitted drying curve underestimates and the fitted wetting curve overestimates the experimental retention data near saturation because n_1 is identical for both curves. While the fitted main loop closes at around $h = -100$ cm, the observed loop closes at around $h = -20$ cm. This disagreement comes from fitting for the entire pressure head range (Fig. 1a). Although certain discrepancies still exist at the beginning and end of the loop, the hysteretic water retention model can describe reasonably well both the drying and wetting retention curves as a whole for Andisols.

Figures 2a and 2b show the main hysteretic loop for two hypothetical soils having different n_1 values. Drying and wetting processes are indicated by the direction of the arrows. Parameters for both hypothetical soils are given in Table 1. The gradient of the water content decrease close to saturation is steeper for n_1 = 2.56, representing a narrower pore-size distribution. On the

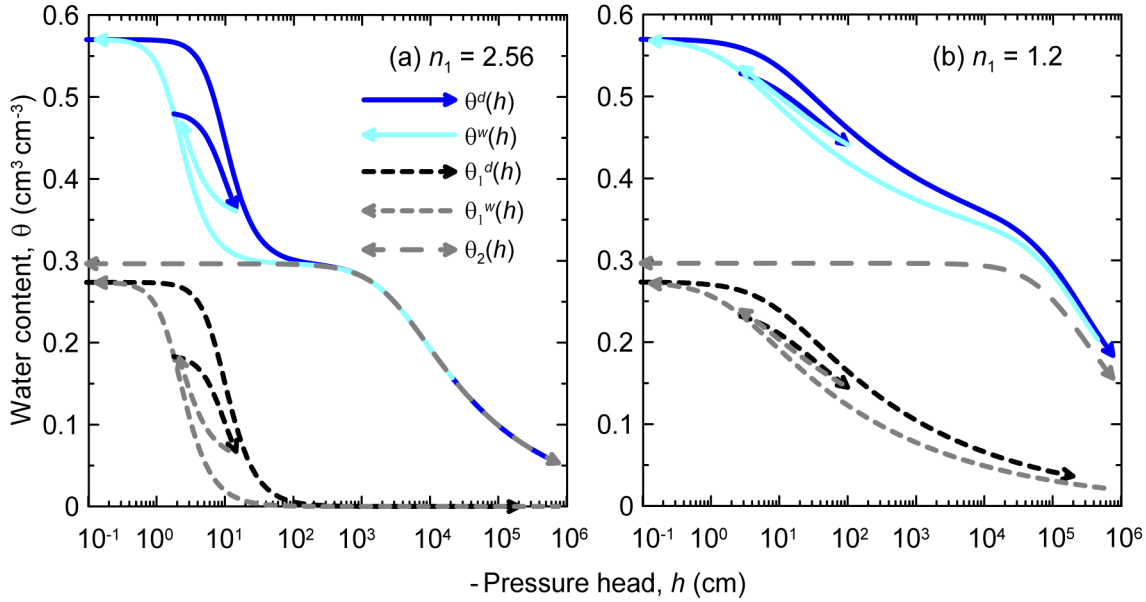

Fig. 2. Main hysteretic loop, primary drying (θ^d) and subsequent wetting (θ^w) scanning curves of $\theta(h)$ for soils with (a) the van Genuchten shape parameter n_1 = 2.56 and (b) n_1 = 1.2. Dashed lines are for retention curves of the two subdomains (denoted by subscripts 1 and 2), solid lines are for the composite retention functions, dark blue lines represent drying curves, and light blue lines represent wetting curves.

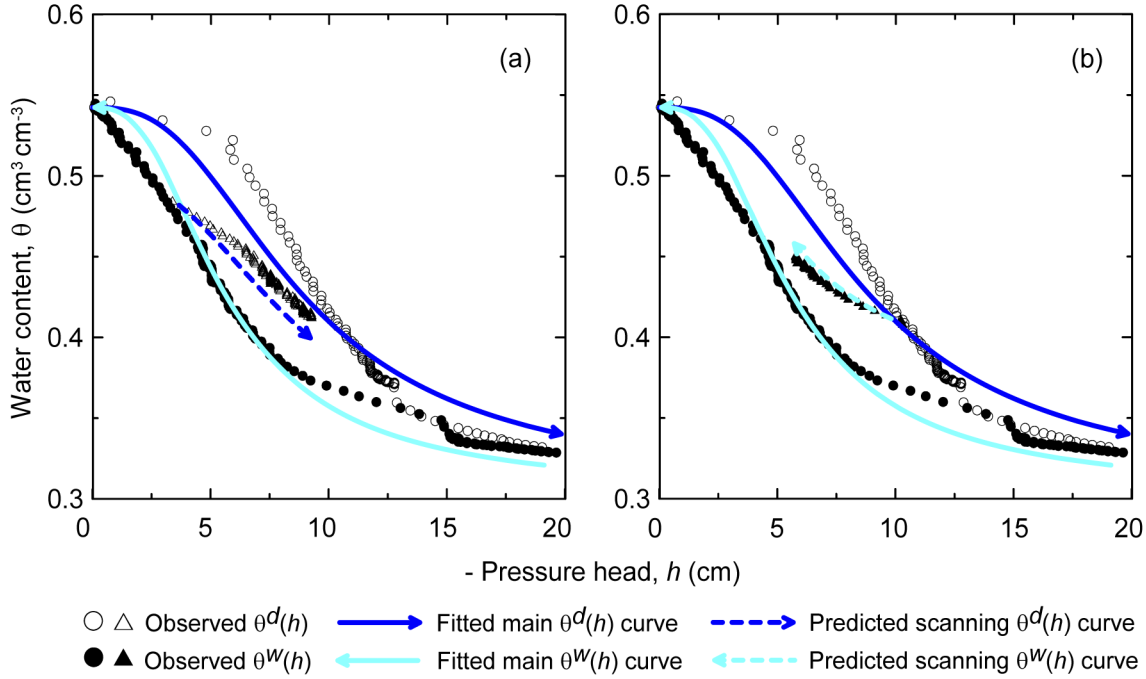

Fig. 3. Main branches of wetting (θ^w) and drying (θ^d) retention curves as shown in Fig. 1b, as well as observed (open and solid triangles) and predicted (dark and light blue dashed lines) scanning curves: (a) drying scanning curve departing from the main wetting curve and (b) wetting scanning curve departing from the main drying curve.

other hand, n_1 = 1.2, reflecting a wider pore-size distribution, results in a smaller gradient.

For n_1 = 2.56, hysteresis appears only in $\theta(h)$ near saturation because $\theta_1(h)$ approaches zero for h < −100 cm (Fig. 2a). As in the case of the unimodal VG model, the larger n_1 results in a greater $d\theta/dh$ gradient near saturation and a distinct air entry. Note that the gradient of the first part of $\theta^d(h)$ is the same as for $\theta^w(h)$ because n_1 is identical for both curves. For n_1 = 1.2, hysteresis also occurs at lower pressure heads, extending even to the second section of $\theta(h)$ because $\theta_1(h)$ decreases gradually with decreasing pressure head, as shown in Fig. 2b. The difference between $\theta^d(h)$ and $\theta^w(h)$ at a certain pressure head, h, is larger for the soil with n_1 = 2.56 than for the soil with n_1 = 1.2.

Scanning Retention Curves

Figure 2 also shows a primary drying scanning curve and a subsequent secondary wetting scanning curve. The reversal points (h_Δ, θ_Δ) used in Fig. 2 are (−1.8 cm, 0.479 m^3 m^{-3}) and (−15.1 cm, 0.360 m^3 m^{-3}) for the soil with n_1 = 2.56 and (−1.8 cm, 0.541 m^3 m^{-3}) and (−100.2 cm, 0.447 m^3 m^{-3}) for the soil with n_1 = 1.2.

Figure 3 presents observed and predicted scanning wetting and drying curves for Andisol. A reversal point for the drying scanning curve in Fig. 3a is (−3.4 cm, 0.485 m^3 m^{-3}), while a reversal point for the wetting scanning curve in Fig. 3b is (−10.3 cm, 0.408 m^3 m^{-3}). A good agreement between the observed and predicted scanning curves can be found especially for the wetting scanning curve (Fig. 3b).

Unsaturated Hydraulic Conductivity

Figure 4 presents the unsaturated hydraulic conductivity, K (dashed lines), as a function of the pressure head, h, and water content, θ, derived from the main drying and wetting water retention curves using Eq. [3]. Parameter values are K_s = 1000 cm d^{-1} and ℓ = 0.5, while the remaining parameters are the same as in the water retention curves in Fig. 2. For both soils, the drying $K^d(h)$ function is larger than the wetting $K^w(h)$ function for the entire range of h. On the other hand, the $K^d(\theta)$ and $K^w(\theta)$ functions are almost identical for high water contents (θ > 0.3 for n_1 = 2.56 and θ > 0.36 for n_1 = 1.2); however, $K^d(\theta)$ is larger than $K^w(\theta)$ for low water contents in both soils.

For high water contents, because S_2 is close to 1 and α_1 is significantly greater than α_2 (Table 1), Eq. [3] can be reduced to

$$K(\theta) \approx K_s \left(w_1 S_1 + w_2\right)^{\ell} \left\{ \left[1 - \left(1 - S_1^{1/m_1}\right)^{m_1} \right] \right\}^2 \quad [15]$$

Hence, K as a function of θ is almost identical for higher water contents, regardless of the α_1 value. Conversely, S_1 becomes close to zero for lower water contents. In this case, Eq. [3] can be reduced to

$$K(\theta) \approx K_s \left(w_2 S_2\right)^{\ell} \frac{\left\{ w_2 \alpha_2 \left[1 - \left(1 - S_2^{1/m_2}\right)^{m_2} \right] \right\}^2}{\left(w_1 \alpha_1 + w_2 \alpha_2\right)^2} \quad [16]$$

Because α_1 remains in the denominator of Eq. [16] and α_1^d is different from α_1^w, unrealistic hysteresis in K as a function of θ occurs between $K^d(\theta)$ and $K^w(\theta)$ for lower water contents. Note that in the case of w_2 = 0 for the unimodal VG model, α_1 in Eq. [3] cancels out and K is independent from α_1 (van Genuchten, 1980).

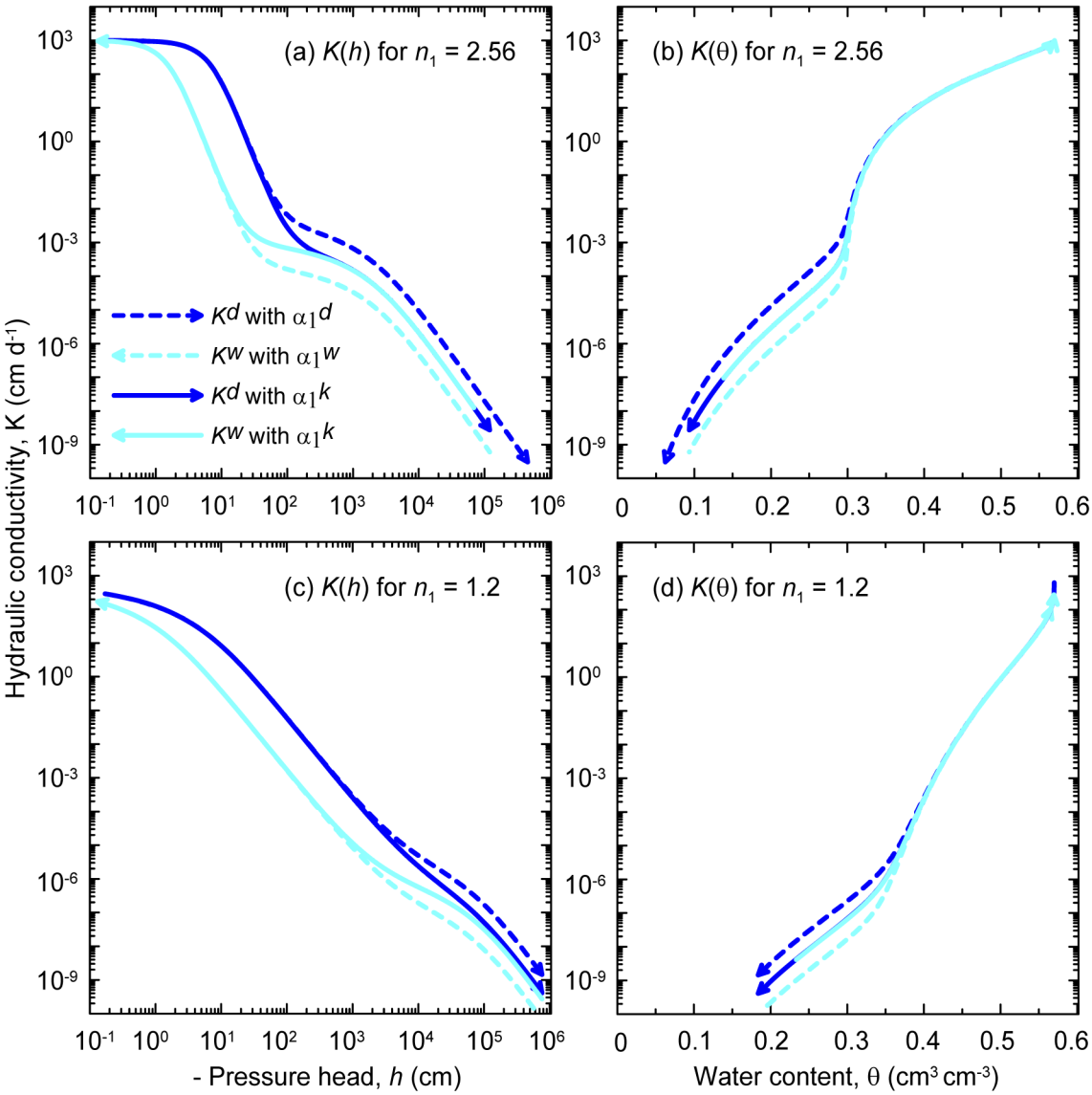

Fig. 4. The unsaturated hydraulic conductivity functions (dashed lines) for the main drying (K^d) and wetting (K^w) water retention curves shown in Fig. 2: (a) $K(h)$ and (b) $K(\theta)$ for the soil with van Genuchten shape parameter $n_1 = 2.56$, and (c) $K(h)$ and (d) $K(\theta)$ for the soil with $n_1 = 1.2$. The $K(h)$ and $K(\theta)$ functions with a single value for the wetting and drying curves combined of the van Genuchten shape parameter $\alpha_1{}^K$ are also plotted as solid lines; dark blue lines represent drying curves and light blue lines represent wetting curves.

The unsaturated hydraulic conductivity is generally assumed to be nonhysteretic when expressed as a function of the water content (van Genuchten, 1980; Mualem, 1986; Plagge et al., 2006). When the K&P model for the unimodal VG model is used, nonhysteretic $K(\theta)$ is obtained using the same n value for both wetting and drying curves (Kool and Parker, 1987). Because $K(\theta)$ is a function of α_1 for the bimodal VG model, as shown in Eq. [16], it is possible to obtain a nonhysteretic $K(\theta)$ function if an additional constraint in terms of a1 in Eq. [3] is imposed. In this study, a single value of $\alpha_1{}^K$ is used for both $K^d(\theta)$ and $K^w(\theta)$, while using $\alpha_1{}^d$ for $\theta^d(h)$ and $\alpha_1{}^w$ for $\theta^w(h)$.

We demonstrate the effects of this additional constraint on the K^d and K^w curves in Fig. 4. For example, the $\alpha_1{}^K$ value is defined here as an average value of $\alpha_1{}^d$ and $\alpha_1{}^w$ on a logarithmic scale, i.e., $\log \alpha_1{}^K = (\log \alpha_1{}^d + \log \alpha_1{}^w)/2$. As shown in Fig. 4a and 4c for both soils (solid lines), $K^d(h)$ is larger than $K^w(h)$ for higher pressure heads, whereas $K^d(h)$ and $K^w(h)$ are almost identical for lower pressure heads. This additional constraint in terms of the $\alpha_1{}^K$ value resulted in an almost nonhysteretic $K(\theta)$ function across the entire range of water contents, as shown in Fig. 4b and 4d.

Although in Fig. 4 we demonstrated the $K(\theta)$ function with an intermediate value of $\alpha_1{}^K$ (between $\alpha_1{}^d$ and $\alpha_1{}^w$), in an ideal case, $\alpha_1{}^K$ would be a fitting parameter obtained from an experimentally determined $K(\theta)$ for low water contents; however, such experimental data are rarely, if ever, available. Further experimental investigations will be needed to evaluate $K(\theta)$ in a relatively dry range.

CONCLUSIONS

We proposed here a hysteretic model of soil hydraulic properties for dual-porosity soils. The model is based on a bimodal

VG model (Durner, 1994) and the K&P hysteresis model (Kool and Parker, 1987). Hysteresis is considered only in the first subregion, $\theta_1(h)$, affecting mainly higher water contents, while a nonhysteretic behavior is assumed in the second subregion, $\theta_2(h)$, affecting mainly lower water contents. The main hysteretic loop is described with $\alpha_1{}^{d}$ for the main drying curve, $\theta_1{}^{d}(h)$, and $\alpha_1{}^{w}$ ($>\alpha_1{}^{d}$) for the main wetting curve, $\theta_1{}^{w}(h)$. The remaining parameter values are the same for the main drying and wetting curves. For soils with a larger n_1 (e.g., n_1 = 2.56), hysteresis affects mainly the first part of the retention curve θ(h) near saturation. On the other hand, for soils with a smaller n_1 (e.g., n_1 = 1.2), some hysteresis extends from full saturation to lower pressure heads, also affecting the second part of the retention curve $\theta(h)$. Scanning curves of $\theta(h)$ can also be successfully described using the K&P model in the first subregion of $\theta_1(h)$. The observed main hysteretic loop and scanning curves for Andisol aggregates could be reasonably well described using this proposed hysteretic model.

The drying and wetting unsaturated hydraulic conductivity functions $K^{d}(\theta)$ and $K^{w}(\theta)$, respectively, are almost identical for higher water contents; however, $K^{d}(\theta)$ is greater than $K^{w}(\theta)$ for lower water contents. To overcome this unrealistic phenomenon in the conductivity function, we use an additional constraint on the value of the α_1 parameter and use a single value $\alpha_1{}^{K}$ for both drying and wetting functions. As a result, an almost nonhysteretic $K(\theta)$ function is obtained for the entire range of water contents. It is necessary to experimentally investigate $K(\theta)$ for low water contents to determine the $\alpha_1{}^{K}$ value.

REFERENCES

Coppola, A. 2000. Unimodal and bimodal descriptions of hydraulic properties for aggregated soils. Soil Sci. Soc. Am. J. 64:1252–1262. doi:10.2136/sssaj2000.6441252x

Diamantopoulos, E., S.C. Iden, and W. Durner. 2012. Inverse modeling of dynamic nonequilibrium in water flow with an effective approach. Water Resour. Res. 48:W03503. doi:10.1029/2011WR010717

Durner, W. 1992. Predicting the unsaturated hydraulic conductivity using multiporosity water retention curves. In: M.Th. van Genuchten et al. (ed.) Indirect methods for estimating the hydraulic properties of unsaturated soils: Proceedings of the International Workshop, Riverside, CA. 11–13 Oct. 1989. U.S. Salinity Lab., Riverside, CA. p. 185–202.

Durner, W. 1994. Hydraulic conductivity estimation for soils with heterogeneous pore structure. Water Resour. Res. 30:211–223. doi:10.1029/93WR02676

Durner, W., and S.C. Iden. 2011. Extended multistep outflow method for the accurate determination of soil hydraulic properties near water saturation. Water Resour. Res. 47:W08526. doi:10.1029/2011WR010632

Fayer, M.J. 2000. UNSAT-H version 3.0: Unsaturated soil water and heat flow model: Theory, user manual, and examples. Pacific Northw. Natl. Lab., Richland, WA.

Kool, J.B., and J.C. Parker. 1987. Development and evaluation of closed-form expressions for hysteretic properties. Water Resour. Res. 23:105–114. doi:10.1029/WR023i001p00105

Kroes, J.G., J.C. van Dam, P. Groenendijk, R.F.A. Hendriks, and C.M.J. Jacobs. 2008. SWAP version 3.2. Theory description and user manual. Alterra, Wageningen, the Netherlands.

Lenhard, R.J., and J.C. Parker. 1989. Modeling multiphase fluid hysteresis and comparing results to laboratory investigations. In: M.Th. van Genuchten et al. (ed.) Indirect methods for estimating the hydraulic properties of unsaturated soils: Proceedings of the International Workshop, Riverside, CA. 11–13 Oct. 1989. U.S. Salinity Lab., Riverside, CA. p. 233–248.

Lenhard, R.J., J.C. Parker, and J.J. Kaluarachchi. 1991. Comparing simulated and experimental hysteretic two-phase transient fluid flow phenomena. Water Resour. Res. 27:2113–2124. doi:10.1029/91WR01272

Miyamoto, T., T. Annaka, and J. Chikusi. 2003. Soil aggregate structure effects on dielectric permittivity of an Andisol measured by time domain reflectometry. Vadose Zone J. 2:90–97. doi:10.2136/vzj2003.9000

Mualem, Y. 1976. A new model for predicting the hydraulic conductivity of unsaturated porous media. Water Resour. Res. 12:513–522. doi:10.1029/WR012i003p00513

Mualem, Y. 1986. Hydraulic conductivity of unsaturated soils: Prediction and formulas. In: A. Klute, editor, Methods in soil analysis. Part 1. 2nd ed. Agron. Monogr. 9. ASA and SSSA, Madison, WI. p. 799–824.

Peters, A., and W. Durner. 2008. A simple model for describing hydraulic conductivity in unsaturated porous media accounting for film and capillary flow. Water Resour. Res. 44:W11417. doi:10.1029/2008WR007136

Plagge, R., G. Scheffler, J. Grunewald, and M. Funk. 2006. On the hysteresis in moisture storage and conductivity measured by the instantaneous profile method. J. Build. Phys. 29:247–259. doi:10.1177/1744259106060706

Priesack, E., and W. Durner. 2006. Closed-form expression for the multimodal unsaturated conductivity function. Vadose Zone J. 5:121–124. doi:10.2136/vzj2005.0066

Schelle, H., S.C. Iden, and W. Durner. 2011. Combined transient method for determining soil hydraulic properties in a wide pressure head range. Soil Sci. Soc. Am. J. 75:1681–1693. doi:10.2136/sssaj2010.0374

Schelle, H., S.C. Iden, A. Peters, and W. Durner. 2010. Analysis of the agreement of soil hydraulic properties obtained from multistep-outflow and evaporation methods. Vadose Zone J. 9:1080–1091. doi:10.2136/vzj2010.0050

Schindler, J., W. Durner, G. von Unold, and L. Müller. 2010. Evaporation method for measuring unsaturated hydraulic properties of soils: Extending the measurement range. Soil Sci. Soc. Am. J. 74:1071–1083. doi:10.2136/sssaj2008.0358

Scott, P.S., G.J. Farquhar, and N. Kouwen. 1983. Hysteresis effects on net infiltration. In: Advances in infiltration: Proceedings of the National Conference, Chicago, IL. 12–13 Dec. 1983. ASAE Spec. Publ. 11-83. Am. Soc. Agric. Eng., St. Joseph, MI. p. 163–170.

Šimůnek, J., M. Šejna, H. Saito, M. Sakai, and M.Th. van Genuchten. 2008a. The Hydrus-1D software package for simulating the movement of water, heat, and multiple solutes in variably saturated media. Version 4.0. HYDRUS Softw. Ser. 3. Dep. of Environ. Sci., Univ. of California, Riverside.

Šimůnek, J., M.Th. van Genuchten, and M. Šejna. 2008b. Development and applications of the HYDRUS and STANMOD software packages and related codes. Vadose Zone J. 7:587–600. doi:10.2136/vzj2007.0077

Steinberg, S.L., G.J. Kluitenberg, S.B. Jones, N.E. Daidzic, L.N. Reddi, M. Xiao, et al. 2005. Physical and hydraulic properties of baked ceramic aggregates used for plant growth medium. J. Am. Soc. Hortic. Sci. 130:767–774.

van Genuchten, M.Th. 1980. A closed-form equation for predicting the hydraulic conductivity of unsaturated soils. Soil Sci. Soc. Am. J. 44:892–898. doi:10.2136/sssaj1980.03615995004400050002x